THE JOURNAL OF PHYSICAL CHEMISTRY B

Article

pubs.acs.org/JPCB

Directed Self-Assembly of Colloidal Model Systems on Charge-Selective Surfaces in External Electric Fields: Theory and Numerical Analysis

Guido Falk*

Department of Powder Technology of Glass and Ceramics, Saarland University, Saarbruecken, Germany

Supporting Information

ABSTRACT: Membrane electrophoretic deposition has a long-established reputation in delivering high quality nanoparticle compact and coating solutions in the field of high performance nanoparticle architectures made from aqueous nanoparticle suspensions. Although for a long time, it has been common practice in nanoparticle science and particle-based nanotechnology to use membrane electrophoretic shaping of nanoparticles, little is known about long-range electrohydrodynamic manipulation of the engineered assembly of colloidal particles at the nanoscale. Here, we analyze the interfacial field-induced flow of a strong electrolyte and its implications for the directed self-assembly of colloidal nanoparticles on nonuniform charge-selective ion-exchange membrane surfaces as well as on conducting microelectrodes imposed to electrophoretic deposition boundary conditions. Numerical calculations of the vortex streamlines are derived for the case of extreme diffusion limitation, concentration polarization near the limiting current, and induced electric forces acting upon the residual space charge. The system is modeled by coupled mass balances, Ohmic law, Navier−Stokes, and Nernst−Planck equations. Particularly, numerical calculations under bulk electroconvection conditions show that the latter provides an efficient intrinsic interfacial mechanism capable of accounting for the experimentally observed local electrophoretic deposition behavior of nanoparticles at ideal permselective membranes with nonplanar periodic charge discontinuity and metal microelectrodes.

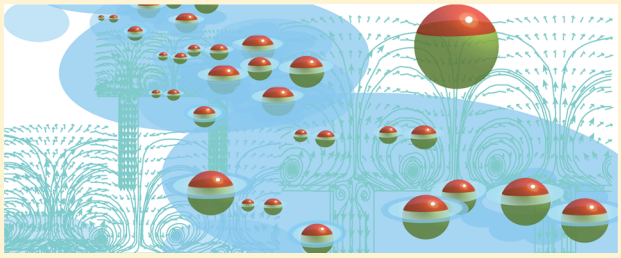

INTRODUCTION

The use of DC and AC external electric fields has been investigated for many years in nanotechnology. External electric-field-directed nanoparticle synthesis processes,[1−4] motion and precipitation of suspensions and bubbles in water,[5−7] suspension filtration characteristics,[8] spray-coating characteristics,[9,10] drying rates of wet-coated layers,[11,12] nanoparticle deposition processes,[13−17] and sintering of ceramic nanoparticles[18,19] have been previously studied. These findings provide comprehensive tools for tailoring specific processing routes of functional and structural nanoceramic materials in applications ranging from lightweight and high-temperature-resistant engineering ceramics, bioceramics, electroceramics, and optoceramics to ceramic microstructures for electronics and sensor applications.

In general, self-assembly means the spontaneous self-organization of nanoparticles due to the combination of specific interactions; for example, interparticle forces or specific external material processing conditions given, for example, by templating or external fields.[20] As an essential part of nanotechnology, the concept of directed self-assembly covers 2D and 3D arrangement of building blocks into ordered, macroscopic structures under appropriate conditions of external fields and combinations of field effects.[21] These external field effects are so far restricted to electric and magnetic fields, flow fields, and the combinations thereof. Building blocks of directed self-assembly methodologies comprise mainly molecules, macromolecules, colloidal particles, nanoparticles, and DNA proteins.

The most crucial issue of research subjects in micromanipulation and directed assembly of colloids and nanoparticles by electric fields is the development of a fundamental understanding of the most powerful combinations of influencing factors controlling external-field-directed assembly of nanoparticles and colloids. The fundamental principle involved in electric-field-directed self-assembly of ordered colloidal structures uses the destabilizing effects of electric fields on dielectric interfaces by induction of polarization due to an electric field and vice versa, induced electric field changes, and field-induced electrokinetic flow of colloids and particles[22,23] as well as electrohydrodynamic flow of the liquid phase.[24−30] These destabilizing effects of local anisotropic, asymmetric, and anisometric electrified interfaces among electrodes, substrates, particles, and electrolytes affect, among others, local changes of surface tension;[31,32] resistivity and permittivity; double layer constitution; ζ-potential;[33] charge

Special Issue: Electrophoretic Deposition

Received: May 14, 2012
Revised: August 13, 2012
Published: August 22, 2012

   dx.doi.org/10.1021/jp304672t | J. Phys. Chem. B 2013, 117, 1527−1536

density; interfacial ion concentration distribution; and, most specifically, electroosmotic flows.

Well-known fluid dynamic models for the calculation of electroosmotic flows are based on the assumption that the solid surfaces are nonpolarizable. The ζ-potential intrinsically describes the surface charge, defined by the surface charge density of immobile surficial charge carriers.[34,35] Provided that the solid surfaces are polarizable, these conditions are not present, since the polarization has a significant influence on the ζ-potential, which is not negligible. This particularly applies in the case of electroosmotic flows about metal electrodes,[36−38] permeable membranes,[39−43] and porous particles.[44,45] There is already intensive work on modeling of electrokinetic flows about ideally polarizable surfaces, especially with respect to spherical particles,[46−50] and microfluidic applications.[51−54]

Studies carried out to model comparable fluid dynamics about dielectric surfaces have been sporadic.[55] Important studies[46,56] have made it clear that polarization of dielectric surfaces at the microscale and polarization of ideally conducting surfaces at the macroscale result in equivalent electroosmotic flows. These findings provide an important basis for understanding how electrokinetic effects influence fluid dynamic transport phenomena about sharp corners,[57] electrophoretic motion of nonspherical particles,[56,58] and transient electrokinetic charging.[59] These models have also been extended to reflect nonlinear macroscopic flows about polarizable solid surfaces.[60]

Recent experimental studies illustrate the particular importance of induced local anisotropic, asymmetric, and anisometric charge distributions on interfaces as probably one of the most powerful fundamental mechanisms of particle patterning under external electric field conditions. Particles with two hemispheres of different polarizabilities or charges were assembled to form monolayers with chainlike structures under AC electric field conditions.[61,62]

Multiple electrohydrodynamic forces acting on a particle near an electrode under AC field conditions have been analyzed by TIR microscopy.[63,64] In another work, colloidal cluster formation of different shapes under AC field conditions is argued to depend on local anisotropic, asymmetric, and anisometric electric field distributions and local surface heterogeneities, causing distinct hydrodynamic flow that causally justified the different shapes of clusters formed.[65]

On the basis of these investigations, it became clear that the resulting forces acting on the particle originate from the gradient of electrohydrodynamic pressure around the particle and from the dielectric force induced by the conductivity gradient.[66] It is considered verified that anisotropic, asymmetric, and anisometric charge characteristics of local interfaces result from at least two local zones of different dielectric characteristics and different polarizabilities causing this interfacial electrostatic pressure. The resulting destabilization of the interfacial zone has been shown to result in the formation of combinations of restoring forces that make pattern formation processes possible,[67] on the condition that the interaction energies causing particle patterning are significantly greater than the thermal energy, kT.

A more detailed understanding of the synergy among complex interactions and processes of polarization, electric field induction, electrokinetic colloid and particle motion, and electrohydrodynamics of fluid flow is of technological importance. In applications including 2D and 3D patterning of nanoparticles, the ability to control directed assembly of nanoparticles and colloids by external electric fields is crucial.

When applied materials science aspects are considered, implications of field-directed self-assembly of colloidal crystals affect the processing of (3D) photonic crystals,[68−70] templates for fabrication of inverse opals[71] and opal films,[72] nanostructured biosensors and bioelectronics,[73] and complex structures and patterned (2D) monolayer arrays of colloidal microspheres.[74,75]

This paper is organized as follows: First, the standard electrokinetic theory of nonlinear electroconvective instability at charge-selective ion exchange membranes is derived in the context of the flow of strong electrolytes at moderate concentrations. The resulting EHD flow induced by electroosmosis of the second kind is then revisited via the numerical solution of the full nonlinear system of equations, derived for the case of overlimiting conduction. The size of the family of calculated flow streamline vortices is on the order of the diffusion layer width for infinitely extended membrane surfaces.

Next, a mathematical model for simulating EHD flow patterns at charge-selective ion-permeable surfaces with surficial charge discontinuities is derived. The system is modeled by coupled mass balances, Ohmic law, Navier−Stokes, and Nernst−Planck equations. The previous derived theory of convective electrodiffusion induced by electroosmotic slip is included by the replacement of a thin electric double layer with the Helmholtz−Smoluchowsky relation between the electroosmotic velocity and the tangential component of the electric field. In a next step, the numerical model is transferred to a microelectrode arrangement. The charge discontinuity is realized by a micrometer-sized ideally conducting metal phase incorporated in an ideally isolating boundary.

Next, to test the applicability of the fundamental theory and the derived mathematical model of electrophoretic deposition of colloidal particles in an external electric field, we report verified and representative current−voltage curves of DC membrane electrophoretic deposition processes to confirm the assumptions of concentration polarization, overlimiting current conditions, and EHD flow patterns affect particle deposition behavior.

Finally, to test the model under AC conditions for the underlying microelectrode arrangement, we consider electrohydrodynamically induced trapping of nanometer-sized particles by video microscopy. The consistency of a theoretically calculated particle pattern and the experimentally observed microstructure can be harnessed in a principal electrophoretic 2D and 3D particle patterning mechanism.

THEORY

Governing Equations. The theory is based on the time-dependent overlimiting conductance ion transfer in the quasielectroneutral diffusion layer $(-\infty < x < \infty, 0 < y < 1)$ at a permselective solid/liquid interface set out by Rubinstein et al.,[76]

$$\left(1 + \frac{1}{D}\right)(c_t + Pe\mathbf{v}\vec{\nabla}c) = 2\vec{\Delta}c \tag{1}$$

$$-\mathbf{v} = u\mathbf{i} + w\mathbf{j} \tag{2}$$

$$\frac{1}{Sc}\mathbf{v}_t = -\vec{\nabla}p + \vec{\Delta}\mathbf{v} \tag{3}$$

$$\vec{\nabla}\mathbf{v} = 0 \tag{4}$$

dx.doi.org/10.1021/jp304672t | J. Phys. Chem. B 2013, 117, 1527−1536

The boundary conditions of the outer edge of the diffusion layer, corresponding to a specific bulk concentration, vanishing normal velocity and no shear, are $(y = 1)$

$$c|_{y=1} = 1 \tag{5}$$

$$u|_{y=1} = 0 \tag{6}$$

$$w|_{y=1} = 0 \tag{7}$$

The specific boundary conditions for electroosmosis of the second kind are $(y = 0)$

$$c|_{y=0} = 0 \tag{8}$$

$$w|_{y=0} = 0 \tag{9}$$

$$u|_{y=0} = -\frac{1}{8}V^2 \frac{\frac{\partial^2 c}{\partial x\,\partial y}}{\frac{\partial c}{\partial y}}\bigg|_{y=0} \tag{10}$$

Here, Sc is the Schmidt number, Pe is the Peclet number, c_t is the time-dependent ion concentration, D is the ionic diffusivity, $\mathbf{v}$ is the fluid velocity, c is the dimensionless ionic concentration, p is pressure, and V is the applied voltage. The reformulation of the spectral problem and Fourier transformation results in the solution of the boundary value problem according to[76]

$$-\frac{\lambda}{PeC\sinh k} = \frac{\lambda_1 \coth \lambda_1}{Sc - 1} + k\coth k - \frac{Sc\lambda^*\coth \lambda^*}{Sc - 1} \tag{11}$$

where

$$\lambda^* \overset{\text{def}}{=} \sqrt{k^2 + \lambda/Sc}, \qquad \lambda_1 \overset{\text{def}}{=} \sqrt{\lambda\frac{D+1}{2D} + k^2} \tag{12}$$

and

$$C = -\frac{k^2 a \sinh \lambda^*}{k\cosh k \sinh \lambda^* - \lambda^* \cosh \lambda^* \sinh k} \tag{13}$$

Here, k is the wavenumber and λ is the spectral parameter.

a and b are in the relevant range ($Pe \sim 1$, $0.1 < D < 10$, $0 < V^2 < 10^4$), and all roots of eq 11 are real. The stability curve is then

$$\frac{1}{8}V^2\frac{Pe(D+1)}{2D} = 4\frac{\sinh k\cosh k - k}{\sinh k\cosh k + k - 2k^2\coth k} \overset{\text{def}}{=} f(k) \tag{14}$$

and the term $(1/8)V^2[(Pe(D+1))/2D] > f(k)$ corresponds to instability.

EHD Flow Model. We consider the local transversal current density, I, of the system with the electric potential, ϕ, and an ideally permselective membrane which is impermeable for counterions:

$$I \overset{\text{def}}{=} (\overline{c}_y + \overline{c}\phi_y) \qquad \text{and} \qquad \overline{c} \overset{\text{def}}{=} c^- = c^+ \tag{15}$$

$$c\phi_y(x, 0) = c_y(x, 0) \tag{16}$$

The slip condition,

$$u_s = -\frac{1}{8}V^2\frac{\frac{\partial^2 c}{\partial x\,\partial y}}{\frac{\partial c}{\partial y}}\bigg|_{y=0} \approx -\frac{V^2}{8}(\ln c)_x\bigg|_{y=0} \tag{17}$$

is rewritten as

$$u_s = -\frac{1}{8}V^2\frac{I_\tau}{I} = -\frac{V^2}{8}\frac{c_{yx}}{c_y}\bigg|_{y=0} \approx -\frac{V^2}{8}(\ln c)_x\bigg|_{y=0} \tag{18}$$

Here, subscript τ denotes differentiation in the lateral direction. According to[76] families of steady state flow streamlines can be calculated for different H values by finite differences in the domain $0 < x < H$, $0 < y < 1$. The vortice size corresponde to the maximal size of the considered box width, and for infinite extended lateral layer, the size of the vortice is on the order of the diffusion layer width.

According to this theory, ideally permselective membranes show different current densities in adjacent regions. Within the regions of extreme concentration polarization, higher current density and nonlimiting conductance the potential drop is smaller compared with the region of lower current density. The resulting EHD flow is directed toward the higher current density region. Consequently, transport of ionic species is directed toward regions of higher potential gradients. The electric field is a consequence of two adjacent regions with different current densities and is not applied externally.

The scheme of the resulting EHD vortex flow at permselective membranes under overlimiting conductance conditions is given in Figure 1.

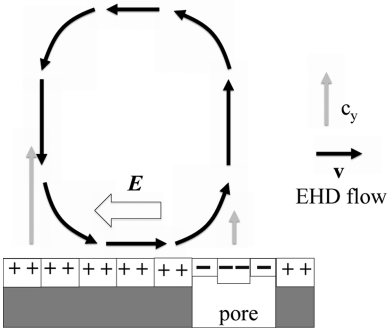

Figure 1. Scheme of the principal mechanism of the formation of EHD vortex instabilities at permselective membranes under overlimiting conductance conditions.

FEM Representation. *Mathematical Model.* A two-dimensional spatial domain of the intersection of a membrane surface under DC electrophoretic deposition conditions is considered in Figure 2.

The ionic charge concentration immediately in the direct vicinity of the porous area is causing a charge discontinuity, which results in a lateral electrical potential gradient and an effective electrical field strength in the tangential direction relative to the membrane surface. To be able to model the fluid flow and ion particle transportation immediately at the pore site, the scale of the geometry is adapted to the range of the Debye length of the considered membrane surface. In this specific case, the transport and interaction processes initiated by the Debye layers of all boundaries are replaced by a finite tangential slip velocity following from the Helmholtz–Smoluchowski relation:

dx.doi.org/10.1021/jp304672t | J. Phys. Chem. B 2013, 117, 1527–1536

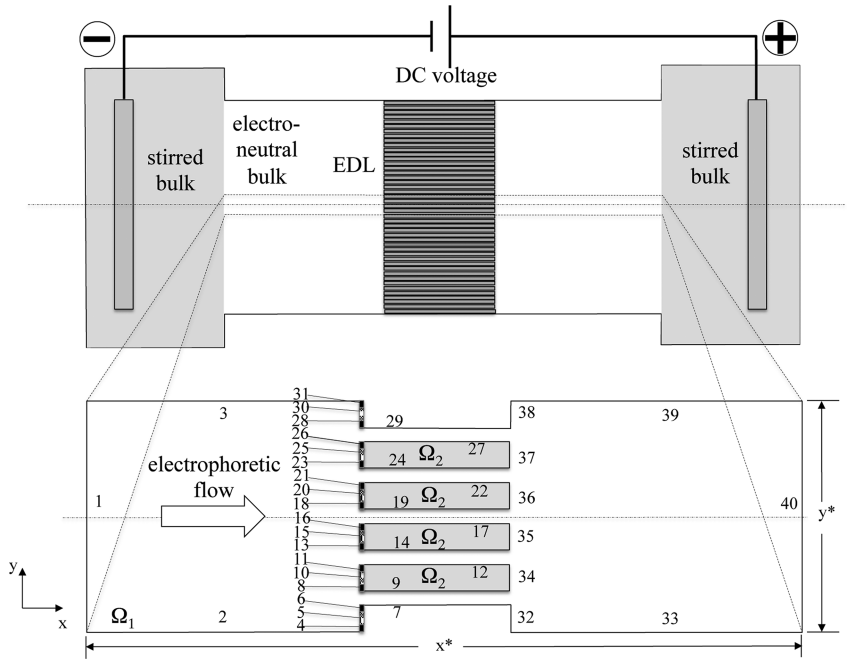

Figure 2. Schematic of the microfluidic model of membrane electrophoretic deposition. The membrane surface is represented as a charge-selective solid. Anions of the electrolyte are supposed to penetrate the permselective membrane. Charge discontinuities are indicated by a negative charge of the membrane pores and a positive charge of the nonporous membrane surface sections. The domain Ω_1 is the electrolyte phase, Ω_2 is the solid dielectric bulk phase of the membrane. The geometry was restricted by setting the length, x^*, and the width, y^*, of the cell such that $x^* = 800$ nm and $y^* = 300$ nm.

$$v_t = -\frac{\varepsilon\zeta}{\eta}E_t \tag{19}$$

Considering these simplified conditions ($\lambda_D = 0$) and local stoichiometric electroneutrality, the fundamental equations can be solved. In this case, the so-called bulk solution of convective electrodiffusion transport is attained. Due to the assumed electroneutrality, the right side of the Poisson equation can be neglected,

$$\vec{\nabla}^2\,\phi(r, t) = 0 \tag{20}$$

and the distribution of the electrical potential is given by the Laplacian. At the same time, the electrical volume force disappears in the Navier–Stokes equation, and finally, the balance equation of the ionic components has to be solved. It has to be noted that this model is based on a charge discontinuity in the area of the membrane pore without the influence of any external potentials.

Problem formulation. Under local considerations, the Ohmic law can be written with the vectorial current density field **E**, the field with the electrical field strength E, and the proportionality factor σ in the form:

$$\mathbf{J} = \sigma\mathbf{E} \text{ and } E = -\vec{\nabla}\phi \tag{21}$$

In the stationary case without any concentration gradients of the charge carrying ions, it follows that

$$-\nabla\cdot(\sigma\vec{\nabla}\phi) = 0, \quad \mathbf{x} \in \Gamma_{\text{Pore}} \tag{22}$$

Thereby, the surficial boundary section in direct vicinity of the membrane pores causes the charge discontinuity with the potential V_0 and $-V_0$. The boundary condition for isolating interfaces is

$$-\sigma\vec{\nabla}\phi\cdot\mathbf{n} = 0, \quad \mathbf{x} \in \Gamma_{\text{Isolation}} \tag{23}$$

Other fundamental boundary conditions concern the Nernst–Planck equation describing the ion concentration, c_i; the ion diffusivity, D; and the flow velocity, **v**, by neglecting migrative transport contributions:

$$\frac{\partial c}{\partial t} + \vec{\nabla}\cdot(-D\vec{\nabla}c_i + c_i\mathbf{v}) = 0, \quad \mathbf{x} \in \Omega_1 \tag{24}$$

The Navier–Stokes equation and the mass continuity equation are given by the following equations if the electrostatic volume forces are neglected:

$$\rho\left(\frac{\partial\mathbf{v}}{\partial t} + \mathbf{v}\vec{\nabla}\cdot\mathbf{v}\right) = \eta\vec{\nabla}^2\mathbf{v} - \vec{\nabla}p, \quad \mathbf{x} \in \Omega_1, \tag{25}$$

$$\vec{\nabla}\cdot\mathbf{v} = 0, \quad \mathbf{x} \in \Omega_1 \tag{26}$$

On the basis of these fundamental equations, the spatial and temporal field variables of the following quantities can be calculated:

$$c_i(t, \mathbf{x}), \quad \phi(t, \mathbf{x}), \quad \mathbf{v}(t, \mathbf{x}), \quad p(t, \mathbf{x}) \tag{27}$$

Hereby, these quantities are

$$c_i(t, \mathbf{x}), \quad \mathbf{x} \in \Omega_1, \tag{28}$$

the molar concentration of the ion component i,

$$\phi(t, \mathbf{x}) = \begin{cases} \phi_1(t, \mathbf{x}) & \mathbf{x} \in \Omega_2 \\ \phi_2(t, \mathbf{x}) & \mathbf{x} \in \Omega_2 \end{cases} \tag{29}$$

the electrical potential,

$$\mathbf{v}(t, \mathbf{x}) = (u(t, \mathbf{x})), v(t, \mathbf{x})) \tag{30}$$

the vectorial field of the fluid flow, and

dx.doi.org/10.1021/jp304672t | J. Phys. Chem. B 2013, 117, 1527–1536

$$p(t, \mathbf{x}) \quad \mathbf{x} \in \Omega_1 \tag{31}$$

the pressure. Furthermore, it is assumed that the electrolyte cell contains an electrolyte of the molar concentration $c_0 = 1 \times 10^{-3}$ mol/L . At stationary conditions ($t = 0$), it is assumed that an osmotic laminar flow, U_0, is initiated with a velocity of 0.1 mm/s. This osmotic flow is characterized by the flow direction from the right to the left section of the cell. The relative permittivity of the electrolyte, ε_r, is 80.2; the ζ-potential is −100 mV; and the maximum potential of the membrane surface is $V_0 = 100$ mV. The ion diffusivity, D, is $1{\cdot}10^{-10}$ mm^2/s. The univalent electrolyte in the suspension cell ($z = 1$) is characterized by the electrical conductivity, $\sigma_w = 1.2{\cdot}10^{-2}$ S/m. The dynamic viscosity, η, and the density, ρ, are assumed to be constant ($\eta = 1{\cdot}10^{-3}$ Pa·s, $\rho = 10^3$ kg/m^3). The electrical boundary conditions at the solid/liquid interfaces with the exception of the potential carrying intersections are

$$-\sigma_w \vec{\nabla}\phi \cdot \mathbf{n} = 0, \quad \mathbf{x} \in \Gamma_{\text{Isolation}} \tag{32}$$

For the potential-carrying intersections of the membrane, the boundary conditions is

$$\phi(t, \mathbf{x}) = \begin{cases} V_0(t, \mathbf{x}) & \mathbf{x} \in \Omega_2, \\ -V_0(t, \mathbf{x}) & \mathbf{x} \in \Omega_2 \end{cases} \tag{33}$$

The concentrated electrolyte solution of the electrolyte cell with the concentration c_0 is assumed to enter the system by laminar flow through the open boundary 40. Under stationary conditions ($t = 0$, $V_0 = 0$), the electrolyte leaves the system pressureless ($p = 0$) through the open boundary 1 under the assumption of convective flow conditions:

$$\mathbf{n}(-D\vec{\nabla}c) = 0 \tag{34}$$

For all other boundaries, bearing no potential and attaining no open boundary conditions for in- and outflow of electrolyte, the thin EDL is replaced by the Helmholtz−Smoluchowski equation given above. At these interfaces, no charge gradients should be initiated, and the boundary conditions are

$$\mathbf{v} = \frac{\varepsilon_w \zeta}{\eta} \vec{\nabla}_T \phi \tag{35}$$

$$0 = \mathbf{n}(-D\vec{\nabla}c + c\mathbf{v}) \tag{36}$$

Numerical Analysis under DC Conditions. The numerical algorithm was implemented in the commercial software program COMSOL Multiphysics 3.5 (Femlab). The Femlab procedures use the method of finite elements for discretization of the domains Ω. In this case, mesh discretization resulted in 11 200 continuous triangular subdomains. The smallest discretization level of about 0.05 of the characteristic Debye length, λ_D, was used near to the surficial subdomains carrying the surface potential, since within these subdomains, the largest gradients of the field variables have been expected. In the case of stationary analysis ($t = 0$), the linear solution algorithm PARDISO was used. The numerical solution of the Navier−Stokes and Nernst−Planck equations for transient conditions ($t > 0$) was achieved by the BDF algorithm. To investigate the flow structure around ion concentration inhomogeneities, the system applies a time-dependent electric field, owing to the unstationary case of nonlinear electroosmosis. The electric field is modeled as the product of a stationary electric field and a time-dependent phase factor $\sin(\omega t)$. The transient solution for the incompressible Navier−Stokes and the convection and diffusion application modes are obtained from the initial state of the of the electric potential field (DC solution at $t = 0$) using a stationary solver. A typical instantaneous streamline pattern is shown in Figure 3.

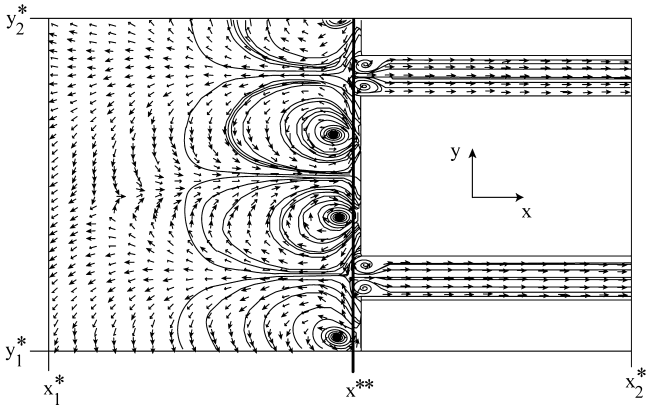

Figure 3. Streamlines for EHD flow at a permselective membrane surface subject to a time-dependent tangential electrical field owing to nonlinear electroosmotic flow conditions. The spatially oscillatory perturbation is expressed in two counter-rotation rolls with flow direction toward the membrane surface within the intersection between the membrane pores. The flow is directed toward the bulk electrolyte within the pore intersections. Arrows indicate flow direction. The dimension of the studied geometry (dimension of the geometric parametric space) was set to (x_1*, x_2*; y_1*, y_2*) = (160, 130, 200 nm). The absolute pore diameter is set to 10 nm; the value x** is set to 248 nm.

The pairs of vortices form counter-rotating rolls with the flow directed toward the region of the nonporous membrane surface section. Within the region of the membrane pores, the electroosmotic recirculation is directed toward the bulk electrolyte phase. The variations of x- and y-components of the velocities induced by electroosmotic slip and electric field are given in Figure 4. In this particular case, the dimensions of the studied geometry (x_1*, x_2*; y_1*, x_2*) were set to (245, 245; 0, 70 nm). We restrict the analyzed geometry by setting the width, w, of the geometry to $w = 70$ nm. The lateral dimension of the permselective membrane scales with the value $\tilde{y} = (y/w)$. The perturbation of the flow is initiated by the resulting electroosmotic flow in the direction tangential to the permselective membrane surface.

Keeping in mind that Figure 3 describes the 2D flow field of the electroosmotic flow, note that each point of the field is defined by scalar quantities at given x- and y-coordinates, respectively. Here, the membrane surface is located at the x-coordinate x_M* = 250 nm. To study electroosmotic flow velocities and electric field components quantitatively at a distance of 2 nm above the membrane surface, a constant x-coordinate at x** = 248 nm is considered (see Figure 3). In Figure 4 a and b, the x and y quantities of the flow field and the electric field at the local coordinate x** = 248 nm = const are given. Referring to the dimensions of the flow field shown in Figure 3, it should be mentioned that the considered membrane surface element is restricted to the length scale y_1* = 130 nm and y_2* = 200 nm, because the x and y quantities of the considered fields vary periodically in accordance with the periodic arrangement of the charge-carrying nanopores of the membrane.

dx.doi.org/10.1021/jp304672t | J. Phys. Chem. B 2013, 117, 1527−1536

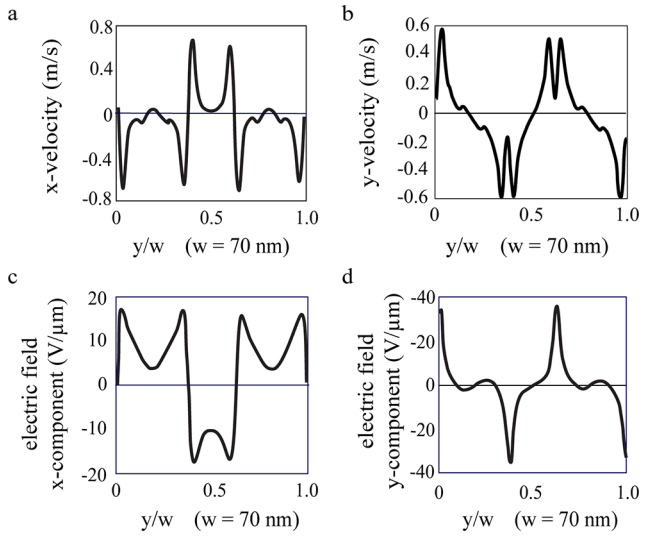

Figure 4. Tangential and orthogonal velocities of the liquid electrolyte phase at a distance of Δx = 2 nm = const above the surface of a permselective nanoporous membrane with surficial charge discontinuities (a, b). The width, w, of the analyzed membrane surface section is 70 nm. The absolute y-coordinates of the analyzed system geometry are y_1* = 130 nm and y_2* = 200 nm at x** = 248 nm = const. Tangential and orthogonal electric field components. The induced tangential electrical field results in major lateral pressure drops owing to the lateral variations of the tangential velocity fluctuations (c, d).

To discuss the fundamental significance of the membrane nanopores on the electrokinetic flow characteristics, the respective functions of the x- and y-components of the flow velocities and electric fields are considered to be closely correlated with the respective flow field geometry given in Figure 3.

The microvortices are arranged in pairs, but in the opposite direction of rotation, from which the fluctuations of the tangential component of the fluid velocity with marked maxima and minima is determined. The pressureless low flow centers of the microvortice cause a splitting of the maxima and minima. The functions shown are calculated for the coordinate x** = 248 nm = const to describe the fluctuations at a distance of 2 nm above the membrane surface, as it was already mentioned before (see Figure 4). For clockwise rotation of the microvortice, negative tangential flow velocities are obtained; counterclockwise rotation results in positive values of fluid velocities in the y-direction. Within the center of the microvortices, the orthogonal component of the fluid velocity changes in discontinuous jumps. Negative x values of the fluid velocities indicate a fluid flow directed toward the bulk phase of the electrolyte. Positive x-components of the fluid velocity result in a fluid flow directed toward the membrane surface. Near the center of the microvortice, the x-component of the velocity field reaches a minimum, in accordance with the low-pressure and low-flow conditions in this domain. Short-wave humpy curves of the x flow velocities appear near the membrane pores, indicating local surface charge heterogeneities. The FEM solution captures the maximum magnitude of the x- and y-components of the electric field strength in the local domain of the microvortices. Negative y-components indicate clockwise rotation of the microvortice, and positive y-components correlate to counterclockwise rotation. The overlapping maxima of the tangential components of the electric field and of the fluid velocity are proven by these calculations. Near the centers of the microvortices, the x-component of the electric field moves from positive to negative rates and vice versa.

Inside the perturbated aqueous electrolyte solution, the following convection−diffusion equation describes the concentration of dissolved ions and colloidal particles in the fluid according to equation 24:

$$\frac{\partial c}{\partial t} + \vec{\nabla}(-D\vec{\nabla}c) = -\mathbf{v}\nabla c \tag{37}$$

On the basis of the numerical analysis of this equation, the diffusive flux, $D\vec{\nabla}c$, as well as the convective flux, $\mathbf{v}\cdot\vec{\nabla}c$, of dissolved ions and colloidal particles are calculated (see Figure 5a, b).

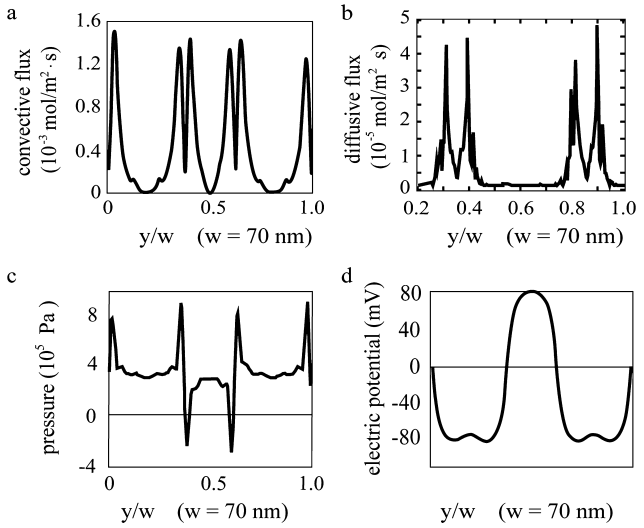

Figure 5. Functions of the convective and diffusive flux densities (a, b) as well as plots of pressure and potential gradients (c, d) at a distance of 2 nm above the surface of a permselective membrane characterized by charge heterogeneities along the x-coordinate; x** = 248 nm = const.

The pressure curve near the membrane surface results from the Navier−Stokes equation (equation 25; see also Figure 5c), and the function of the potential gradient near the membrane surface (Δx = 2 nm, x** = 248 nm = const) is calculated according to equation 22 (see Figure 5d).

The convective flux densities reach their maximum values close to the centers of the microvortices, as expected. The convective flux directly above the membrane pore is negligible. According to these results, deposition of the first particle layer is expected to develop at nonporous surface sites. Compared with these convective flux values, the diffusive flux densities are smaller by nearly 2 orders of magnitude and are significant only near the pore area of the membrane. The numerically proven diffusive transport of charged species across the modeled nanopores is in good agreement with a fundamental understanding of ion transport mechanisms across ion permeable membranes. Pressure gradients are increased close to the centers of the microvortices. Negative pressure gradients correlate to fluid flow directed toward the membrane surface. Positive pressure gradients appear when the fluid flow is directed toward the bulk phase of the electrolyte. Again, the two peaked negative pressure gradients between the two nanopore sections give a reasonable explanation of the

dx.doi.org/10.1021/jp304672t | J. Phys. Chem. B 2013, 117, 1527−1536

preferred particle deposition locations. Finally, the potential near the membrane has its maximum at the membrane pores. A potential of opposite sign is calculated on the interfaces between the charged nanopores, giving a reasonable explanation of the preferred particle deposition at these finite locations. Because the model verifies the assumptions that polarization of the pores of a permselective membrane will yield fluid motion and particle deposition, the influence of the EHD flow on colloidal particle deposition behavior onto charge-heterogeneous permselective membrane substrates is of fundamental interest.To correlate the numerically calculated DC-EHD flow at a permselective membrane with macroscopically measurable effects, a typical current−voltage curve of a DC membrane electrophoretic deposition experiment is considered.

In the case of highly permselective cation exchange membranes, cations penetrate the membrane pores and are separated from the colloidal suspensions. Anion-selective exchange membranes separate anions from the suspension. To focus on the specific aspect of concentration polarization and stationary voltage/current (V−C) curves during membrane EPD, we address charge transfer across anion selective membranes exclusively. The pressure flow of negatively charged ions toward the membrane surface affects the depletion of anions within the colloidal suspension and the accumulation of negatively charged species at the permselective membrane surface. The characteristics of the permselective Nadir cellulose acetate membrane (Fa. Roth Carl GmbH, Art. No. 5104.1) used in the experiments is given in Table 1. The membrane is used for the separation of the setup into a suspension and electrolyte cell according to Clasen.[77]

Table 1. Characteristics of the Permselective Membrane Used for Electrophoretic Deposition Experiments

membrane properties	characteristic values
clycerin concentration	21%
MWCO	10 000−20 000 Da
mean particle size	25−30 rA
total pore surface area	ca. 6%
water vapor permeability (DIN 531122)	100 mg/m^2 bei 20 °C and 85% rel moisture variation
effective diffuse permeability	NaCl: 7−15·10^{-7} cm^2/s (37 °C)
steam-sterilizable at	+130 °C

Flame pyrolytically processed spherical SiO_2 nanoparticles (OX50, Degussa-Evonik) stabilized by tetramethylammonium-hydroxide (TMAH) and suspended in bidistilled aqueous suspensions at solid weight concentration of 45 wt % serves as the model system for membrane electrophoretic deposition under stationary DC voltage conditions. The stationary V−C curve of the membrane electrophoretic deposition experiments is given in Figure 6.

First, it is clear that that voltage/current curve given in Figure 6 relates to the formation of concentration gradients at a permselective solid/liquid interface upon the passage of an electric current, as was observed by Maletzki et al.[78] and numerically experimentally proven by Rubinstein et al.[40−42,79] Accordingly, the low current Ohmic region (region I) is followed by the limiting current region (region II), followed by the overlimiting conductance region (region III). Above a well-defined gating voltage, the overlimiting behavior results in a kind of electroconvective mixing within the depleted diffusion layer near the permselective membrane surface. The gating voltage that correlates to the plateau value of electric current density is usually quantitatively described by the theory of concentration polarization. On the basis of the aforementioned numerical experimental model of electroconvection induced by electroosmotic slip, it is observed that the formation of electrohydrodynamically reasonable microvortices above permselective ion-exchange membranes at overlimiting conductance conditions correlates to the experimentally observed conditions of particle deposition onto the surface of the cellulose acetate ion-exchange membrane (see Figure 6 a, region III). Thus, we cannot exclude the possibility that a cause and effective relationship between the appearance of microvortices near the membrane surface and the deposition of colloidal particles onto the permselective surface might exist.

Numerical Analysis under AC Conditions. We refer to AC electrophoretic deposition experiments carried out by Nold et al.[80] The scheme of electrophoretically driven rapid prototype microstructure deposition consists of a coaxial Pt-microelectrode arranged opposite a permselective membrane-coated Pt plate electrode. The schematic view of the system and a snapshot of the local microvortice streamlines observed in the microcell are given in Figure 7.

The following section will examine the applicability of the above derived numerical model of convective electrodiffusion induced by electroosmotic slip to derive a reasonable explanation of the formed microvortices arranged in pairs with opposing rotatory movement. More importantly, a possible effect of the EHD streamlines on the selective particle deposition behavior found by Nold[80] and a possible influence of the EHD flow on the specific formed microstructure has to be given. It is again emphasized that under these defined boundary conditions, the influence of nonlinear electric double layers and the formation of a space charge layer is neglected. The applied numerical technique therefore requires a quasi-equilibrium behavior of the electric double layer and corresponds to a case of limiting electric currents. In this present instance, the perturbation and charge heterogeneity of the membrane surface of the DC case expressed by a surfacial fluctuation of the surface potential is replaced by the AC voltage attached between the microelectrode and the plate electrode.

The potential-bearing interfaces are characterized by the following boundary condition:

$$\varphi(t, \mathbf{x}) = \begin{cases} -V_0 \sin(\omega t)\ (t, \mathbf{x}) & \mathbf{x} \in \Gamma_{\text{microelectrode}} \\ V_0 \sin(\omega t)\ (t, \mathbf{x}) & \mathbf{x} \in \Gamma_{\text{plate electrode}} \end{cases} \quad (38)$$

The colloidal particle phase is not included in this modeled system, as the EHD flow in the microcell stand at the forefront of attention in this investigation. All other boundary conditions are applied like the one of the DC membrane−EPD case. The streamline pattern of the numerically modeled system is given in Figure 8.

For the most part, the results of the given two-dimensional streamline patterns of the fluid velocities suggest that the counter-rotating microvortice formation observed under video-microscopy conditions can be accounted for accurately by the mathematical numerical approach of convective electrodiffusion induced by electroosmotic slip. The model described reproduces the formation of two other microvortices at a location close to the plate electrode surface at a distance of 2−3d relative to the symmetry line of the considered model

dx.doi.org/10.1021/jp304672t | J. Phys. Chem. B 2013, 117, 1527−1536

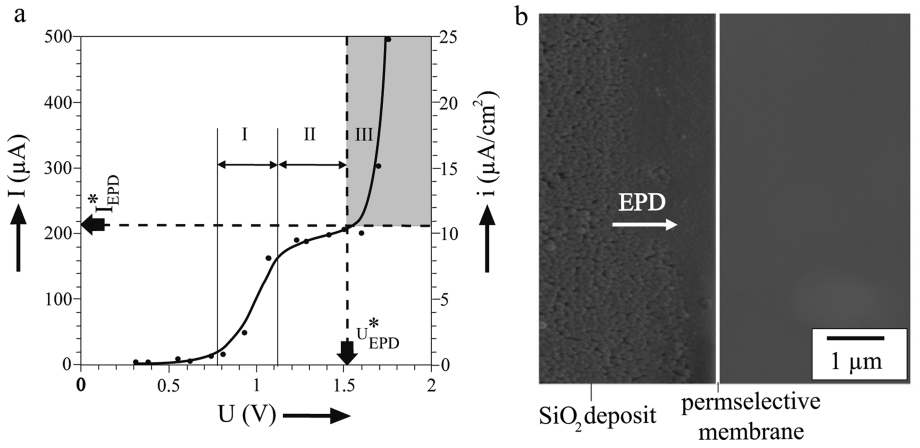

Figure 6. (a) Stationary voltage/current curve of membrane electrophoretic deposition of colloidal SiO_2 nanoparticles suspended in aqueous solutions onto permselective Nadir cellulose acetate membrane (pH = 9.5, σ_{SiO_2} = 1325 μS/cm, TMAH-electrolyte cell with σ_{TMAH} = 15.56 mS/cm). (b) SEM topography of the deposited SiO_2 nanoparticles.

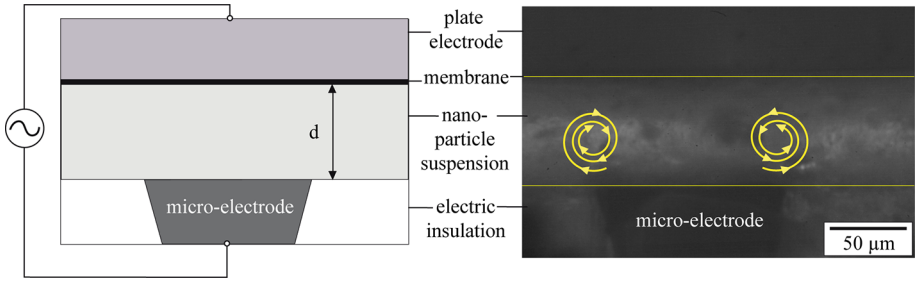

Figure 7. Schematic view of the experimental system realized by Nold et al.[80] (a) In a horizontal microcell, an insulated Pt microelectrode is arranged opposite a permselective membrane-coated Pt plate electrode ($\sigma_{plate\ electrode} = \sigma_{microelectrode} = 6{\cdot}10^7$ S/m, $\sigma_{membrane} = 1.5{\cdot}10^{-3}$ S/m) at a distance d = 100 μm. The asymmetric AC voltage is applied directly to the cell by a function generator with $\phi_1 = -1.9$ V and $\phi_2 = 17.1$ V and f = 450 Hz. The colloidal model system is an α-Al_2O_3 particle suspension (SM8, Baikalox, d_{50} = 300 nm, BET = 10 m^2/g). (b) Videomicroscopic snapshot of the experimental cell showing the streamlines of the microvortices that are formed at both sides of edges of the Pt microelectrode.

geometry. The parameter d refers to the diameter of the microelectrode given to 100 μm.

It has to be stated that according to the numerical calculations, the direction of rotation of the formed microvortices depends on the phase of the applied AC potential that enforces independently of the considered time scale counter-rotation rolls. Consequently, a phase-dependent EHD stagnation point flow of the fluid phase is formed that is directed toward the microelectrode in the case of time scale $\overline{t}_1$ and toward the plate electrode in the case of time scale $\overline{t}_2$ (see Figure 8a, b).

On closer examination of the stationary, time-dependent fluid flow conditions, it becomes obvious that the cyclically controlled application of electrical potential results in an appropriate cyclical attenuation or strengthening of the resulting stagnation point flow behavior of the model system considered. Because of the fast shift of EHD fluid flow behavior initiated by these two center microvortices, no clear particle tracing analysis results of expected particle deposition behavior can be concluded. Because the direction of the dielectrophoretic particle transport depends necessarily on the externally applied phase of the potential, particle movement is directed toward the microelectrode or toward the plate electrode according to these external electric field conditions.

Despite these constraints, particle deposition is observed under formation of a donut-shaped microstructure under these experimental boundary conditions, see Figure 8 c, d. The explanation of the phenomenon of observed donut-shaped microstructure formation under these referred experimental boundary conditions seems to be difficult without including the argumentation of the calculated EHD microvortices formed at the interface of the plate electrode (see Figure 8a, b). The two microvortices that have been numerically calculated at the location close to the interface of the plate electrode can provide an explanation of the observed particle deposition characteristics.

The dynamic and the pressure gradients of the induced microvortices in the vicinity of the plate electrode interface are expected to influence the particle deposition behavior, as was already explained in the DC case. In this way, the induced flow dynamics of the fluid phase influence particle deposition characteristics. These streamline patterns of the interfacial microvortice pair and the induced Maxwell pressure at these interfaces would be a plausible explanation of the experimentally observed deposition characteristics of the model colloidal system. On the basis of these findings and the correlation of numerical and experimental results given in this work, it is postulated that nanoparticles suspended in colloidal suspensions could undergo directed self-assembling, provided the external boundary conditions would allow electrohydrodynamic flow and, more specifically, convective electrodiffusion induced by electroosmotic slip at local selective surface sites. Since directed self-assembled structure formation under different electrophoretic deposition conditions is a promising

dx.doi.org/10.1021/jp304672t | J. Phys. Chem. B 2013, 117, 1527−1536

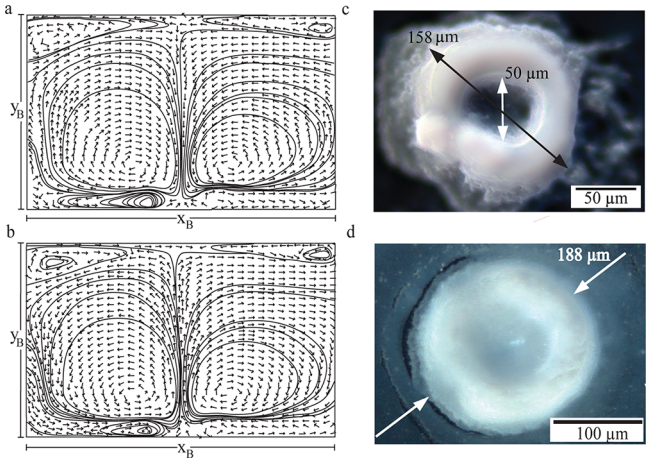

Figure 8. Numerically calculated streamline pattern for EHD flow between an ideally conductive microelectrode and an ideally conductive plate electrode subject to an oscillatory perturbation by the applied AC potential under the assumptions of convective electrodiffusion induced by electroosmotic slip at f = 450 Hz, ϕ_{max} = 17.1 V, and at the time scale (a) $\bar{t}_1$ and (b) $\bar{t}_2$. Counter-rotating microvortices appear above the outer edges of the microelectrodes at locations close to maximum charge heterogeneities and maximum charge density fluctuations. Microstructure of AC-EPD particle deposition according to Nold et al.[80] at f = 450 Hz and ϕ_{max} = 17.1 V (c) and ϕ_{max} = 13.3 V (d). The particle concentration of the colloidal suspension is 16.7 wt %. The deposition time is t = 60 s.

approach to verify the results of the calculated DC- and AC-EHD streamline patterns, respectively, a second part of the is work will report on the experimental verification of the numerical analysis results.

CONCLUSIONS

The two-dimensional membrane EPD model for transient and spatial calculation of the field variables of ion concentration, potential, pressure, and fluid flow velocity explains the microvortice formation that has already been proven experimentally on permselective substrates and conductive metal microelectrodes under AC and DC conditions. Numerical analysis and adoption of the fundamental model equations for interfacial electrohydrodynamic and electrokinetic transport behavior of the fluid phase offer the theoretical investigation of particle deposition mechanisms on a microfluidic scale in the immediate vicinity of heterogeneously charged surfaces. In that way, intrinsic analysis of particle deposition characteristics in aqueous solutions at local sites has been studied theoretically. Computational, FEM-based, fluid dynamics are contributing to a fundamental understanding of particle deposition processes under electrophoretic conditions as far as the boundary conditions are evaluated in relation to the real process conditions. In the specific case of membrane electrophoretic deposition, it is concluded that plausible transient charge dynamics at narrow scales would cause a particle to be deposited at specific selective sites. In the case of AC-EPD, microelectrodes used cause macroscopically comparable microvortices and electrolyte perturbations of specific characteristics that give reasonable explanations of directed field-assisted particle deposition assemblies. The verification of these theoretical results based on experimental DC- and AC-electrophoresis data will follow in a separate study. For future investigations, it is an essential objective to work toward more realistic simulation tools to model the nonlinear boundary conditions influencing particle deposition mechanisms of electrophoretic shaping processes. At the same time, smart experimental techniques for particle tracing analysis at microfluidic boundaries have to be applied.

ASSOCIATED CONTENT

Supporting Information

The entire achemso bundle is generated by running achemso.dtx through TeX. Running LaTeX on the same file will generate the general documentation for both the class and package files. This information is available free of charge via the Internet at http://pubs.acs.org

AUTHOR INFORMATION

Corresponding Author

*E-mail: g.falk@nanotech.uni-saarland.de.

Notes

The authors declare no competing financial interest.

ACKNOWLEDGMENTS

We thank Rolf Clasen and Omer van der Biest for helpful discussions and advice. We gratefully acknowledge internal funding and support from a Powder Technology of Glass and Ceramics Grant, Saarland University, Germany.

REFERENCES

(1) Morrison, P. W.; Raghavan, R.; Timpone, A. J. *Chem. Mater.* **1997**, *9*, 2702−2708.
(2) Suzuki, H.; Nakada, T.; Saito, Y.; Kaito, C. *Jpn. J. Appl. Phys.* **2000**, *39*, 5252−5255.
(3) Katz, J. L.; Hung, C.-H. Initial studies of electric field effects on ceramic powder formation in flames. *23th Symposium (Int.) on Combustion*; pp 1733−1738.
(4) Jiang, G.; Zhuang, H.; Li, W. *Ceram. Int.* **2004**, *30*, 185−190.
(5) Feeley, C. M.; Pohl, H. A. *J. Phys. D: Appl. Phys.* **1981**, *14*, 2129−2138.
(6) Riahifar, R.; Marzbanrad, E.; Raissi, B.; Zamani, C.; Kazemzad, M.; Aghaei, A. *Mater. Lett.* **2011**, *65*, 632−635.
(7) Korobeinikov, S. M.; Melekhov, A. V.; Posukh, V. G.; Antonov, V. M.; Royak, M. E. *High Temp.* **2001**, *39*, 163−168.
(8) Hirata, Y.; Uchima, H.; Tanaka, Y. *J. Am. Ceram. Soc.* **2009**, *92*, S57−S62.
(9) Huneiti, Z.; Balachandran, W.; Machowski, W.; Arnold, P. Harmonic spraying of conducting liquids employing AC-DC electric fields. *IEEE-IAS, Annual Meeting*; pp 1493−1499.
(10) Duby, M.-H.; Deng, W.; Kim, K.; Gomez, T.; Gomez, A. *Aerosol Sci.* **2006**, *37*, 306−322.
(11) Carlon, H. R.; Latham, J. *J. Atmos. Terr. Phys.* **1992**, *54*, 117−118.
(12) Shynkaryk, M. V.; Lebovka, N. I.; Vorobiev, E. *Drying Technol.* **2008**, *26*, 695−704.
(13) Corni, I.; Ryan, M. P.; Boccaccini, A. R. *J. Eur. Ceram. Soc.* **2008**, *28*, 1353−1367.
(14) Neirinck, B.; Fransaer, J.; Biest, O. V. d.; Vleugels, J. *Electrochem. Commun.* **2009**, *11*, 57−60.
(15) Gardeshzadeh, A. R.; Raissi, B.; Marzbanrad, E. *Mater. Lett.* **2008**, *62*, 1697−1699.
(16) Choy, K.-L.; Bai, W. *Depositing films on a substrate using an electric field* **1997**.
(17) Sun, J.; Gao, M.; Feldmann, J. *J. Nanosci. Nanotechnol.* **2001**, *1*.
(18) Müller, M.; Clasen, R. *Ceram. Trans.* **2009**, *209*, 227−236.
(19) Kondo, T.; Kuramoto, T.; Kodera, Y.; Ohyanagi, M.; Munir, Z. A. *J. Ceram. Soc. Jpn.* **2008**, *116*, 1178−1192.
(20) Grzybowski, B. A.; Wilmer, C. E.; Kim, J.; Browne, K. P.; Bishop, K. J. M. *Soft Matter* **2009**, *5*, 1110−1128.

(21) Grzelczak, M.; Vermant, J.; Furst, E. M.; Liz-Marzan, L. M. *ACS Nano* **2010**, *4*, 3591−3605.
(22) Janca, J.; Checot, F.; Gospodinova, N.; Touzain, S.; Sprková, M. *J. Colloid Interface Sci.* **2000**, *229*, 423−430.
(23) López-García, J.; Grosse, C.; Horno, J. *J. Colloid Interface Sci.* **2005**, *286*, 400−409.
(24) Green, N. G.; Ramos, A.; González, A.; Morgan, H.; Castellanos, A. *Phys. Rev. E* **2000**, *61*, 4011−4018.
(25) González, A.; Ramos, A.; Green, N. G.; Castellanos, A.; Morgan, H. *Phys. Rev. E* **2000**, *61*, 4019−4028.
(26) Green, N. G.; Ramos, A.; González, A.; Morgan, H.; Castellanos, A. *Phys. Rev. E* **2002**, *66*, 026305/1−026305/11.
(27) Green, N. G. *Anal. Bioanal. Chem.* **2005**, *382*, 891−893.
(28) Lin, Z.; Kerle, T.; Baker, S. M.; Hoagland, D. A. *J. Chem. Phys.* **2001**, *114*, 2377−2381.
(29) Green, N. G.; Ramos, A.; Gonzalez, A.; Castellanos, A.; Morgan, H. *J. Phys. D: Appl. Phys.* **2000**, *33*, L13−L17.
(30) Saville, D. A. *Phys. Rev. Lett.* **1993**, *71*, 2907−2910.
(31) Morcos, I. *J. Electrostatics* **1978**, *5*, 51−69.
(32) Brodskaya, E. N.; Rusanov, A. I. *Coll. J. USSR* **1983**, *45*, 558−564.
(33) Carrique, F.; Arroyo, F. J.; Delgado, A. V. *J. Colloid Interface Sci.* **2002**, *252*, 126−137.
(34) Mela, P.; Tas, N. R.; Berg, A. v. d.; Elshof, J. E. t. In *Nanofluidics*; Nalwa, H. S., Smalley, R. E., Eds.; American Scientific Publishers, 2004; Vol. *6*, pp 739−755.
(35) Li, D. *Electrokinetics in Microfluidics*; Elsevier Academic Press: Amsterdam, Boston, Heidelberg, London, 2004; Vol. *2*, p 643.
(36) Ramos, A.; Morgan, H.; Green, N. G.; Castellanos, A. *J. Phys. D: Appl. Phys.* **1998**, *31*, 2338−2353.
(37) Ristenpart, W. D.; Aksay, I. A.; Saville, D. A. *Phys. Rev. E: Stat., Nonlinear, Soft Matter Phys.* **2004**, *69*, 021405.1−021405.8.
(38) Ajdari, A. *Phys. Rev. E: Stat., Nonlinear, Soft Matter Phys.* **2000**, *61*, R45−R48.
(39) Rubinstein, I.; Zaltzman, B. *Math. Models Methods Appl. Sci.* **2001**, *11*, 263−300.
(40) Rubinstein, I.; Zaltman, B. *Adv. Colloid Interface Sci.* **2007**, *134*−*135*, 190−200.
(41) Rubinstein, S. M.; Manukyan, G.; Staicu, A.; Rubinstein, I.; Zaltzman, B.; Lammertink, R. G. H.; Mugele, F.; Wessling, M. *Phys. Rev. Lett.* **2008**, *101*, 236101-1−236101−4.
(42) Rubinstein, I.; Zaltzman, B. *Adv. Colloid Interface Sci.* **2010**, *159*, 117−129.
(43) Zaltzman, B.; Rubinstein, I. *J. Fluid Mech.* **2007**, *579*, 172−226.
(44) Ben, Y.; Chang, H.-C. *J. Fluid. Mech.* **2002**, *461*, 229−238.
(45) Ben, Y.; Demekhin, E. A.; Chang, H.-C. *J. Colloid Interface Sci.* **2004**, *276*, 483−497.
(46) Squires, T. M.; Bazant, M. Z. *J. Fluid Mech.* **2004**, *509*, 217−252.
(47) Yariv, E.; Miloh, T. *J. Fluid Mech.* **2008**, *595*, 163−172.
(48) Miloh, T. *Phys. Fluids* **2008**, *20*, 063303-1−063303-12.
(49) Miloh, T. *Phys. Fluids* **2008**, *20*, 107105-1−107105-14.
(50) Miloh, T. *Phys. Fluids* **2011**, *23*, 122002-1−122002-14.
(51) Chang, H.-C.; Yossifon, G. *Biomicrofluidics* **2009**, *3*, 012001-1−012001-15.
(52) Wang, S.; Hu, X.; Lee, L. J. *J. Am. Chem. Soc.* **2007**, *129*, 254−255.
(53) Horiuchi, K.; Dutta*, P. *Lab Chip* **2006**, *6*, 714−723.
(54) Castellanos, A.; Ramos, A.; González, A.; Green, N. G.; Morgan, H. Particle Manipulation in microfluidics: The role of dielectrophoresis, electrohydrodanmcis and ac electrokinetics. *XXI International Congress of Theoretical and Applied Mechanics.*
(55) Saville, D. A. *Annu. Rev. Fluid Mech.* **1997**, *29*, 27−64.
(56) Yossifon, G.; Frankel, I.; Miloh, T. *Phys. Fluids* **2007**, *19*, 068105-1−068105-4.
(57) Yossifon, I., G.; Frankel; Miloh, T. *Phys. Fluids* **2006**, *18*, 117108-1−117108-9.
(58) Yariv, E. *J. Fluid Mech.* **2008**, *613*, 85−94.
(59) Yossifon, G.; Frankel, I.; Miloh, T. *J. Fluid Mech.* **2009**, *620*, 241−262.
(60) Yariv, E.; Davis, A. M. J. *Phys. Fluids* **2010**, *22*, 052006-1−052006-7.
(61) Gangwal, S.; Cayre, O. J.; Velev, O. D. *Langmuir* **2008**, *24*, 13312−13320.
(62) Lumsdon, S. O.; Kaler, E. W.; Velev, O. D. *Langmuir* **2004**, *20*, 2108−2116.
(63) Fagan, J. A.; Sides, P. J.; Prieve, D. C. *Langmuir* **2005**, *21*, 1784−1794.
(64) Hoggard, J. D.; Sides, P. J.; Prieve, D. C. *Langmuir* **2008**, *24*, 2977−2982.
(65) Negi, A. S.; Sengupta, K.; Sood, A. K. *Langmuir* **2005**, *21*, 11623−11627.
(66) Kang, K. H.; Li, D. *J. Colloid Interface Sci.* **2005**, *286*, 792−806.
(67) Morariu, M. D.; Voicu, N. E.; Schäffer, E.; Lin, Z.; Russell, T. P.; Steiner, A. *Nat. Mater.* **2003**, *2*, 48−52.
(68) Norris, D. J.; Arlinghaus, E. G.; Meng, L.; Heiny, R.; Scriven, L. *Adv. Mater.* **2004**, *16*, 1393−1399.
(69) Nakamura, H. *R&D Rev. Toyota CRDL* **2004**, *39*, 33−39.
(70) Prasad, T.; Rengarajan, R.; Mittleman, D. M.; Colvin, V. L. *Opt. Mater.* **2005**, *27*, 1250−1254.
(71) Masuda, Y.; Itoh, T.; Itoh, M.; Koumoto, K. *Langmuir* **2004**, *20*, 5588−5592.
(72) Gu, Z.-Z.; Meng, Q.-B.; Hayami, S.; Fujishima, A.; Sato, O. *J. Appl. Phys.* **2001**, *90*, 2042−2044.
(73) Huwiler, C.; Kunzler, T. P.; Textor, M.; Vörös, J.; Spencer, N. D. *Langmuir* **2007**, *23*, 5929−5935.
(74) Zhang, J.; Li, Y.; Zhang, X.; Yang, B. *Adv. Mater.* **2010**, *22*, 4249−4269.
(75) Winkleman, A.; Gates, B. D.; McCarty, L. S.; Whitesides, G. M. *Adv. Mater.* **2005**, *17*, 1507−1511.
(76) Rubinstein, I.; Zaltzman, B. *Phys. Rev. E* **2000**, *62*, 2238−2251.
(77) Clasen, R. *Electrophoretic Deposition of Compacts of Nanosized Particles*; American Ceramic Society: Westerville, OH, 1995; Vol. *54*.
(78) Rubinstein, I.; Maletzki, F. *J. Chem. Soc. Faraday Trans.* **1991**, *87*, 2079−2087.
(79) Rubinstein, I.; Zaltzman, B.; Lerman, I. *Phys. Rev. E* **2005**, *72*, 011505-1−011505-19.
(80) Nold, A. Ph.D. Thesis, Universität des Saarlandes, 2012.